MOLECULAR IMAGING AND BIOLOGY

Published Online: 3 June 2010
Mol Imaging Biol (2011) 13:342–347
DOI: 10.1007/s11307-010-0347-4

RESEARCH ARTICLE

Image-Derived Input Function from Cardiac Gated Maximum a Posteriori Reconstructed PET Images in Mice

Landon W. Locke,[1] Stuart S. Berr,[1,2] Bijoy K. Kundu[2]

[1]*Department of Biomedical Engineering, The University of Virginia, P.O. Box 801339, 480 Ray C Hunt Drive, Snyder Building, Charlottesville, VA 22908, USA*
[2]*Department of Radiology, The University of Virginia, P.O. Box 801339, 480 Ray C Hunt Drive, Snyder Building, Charlottesville, VA 22908, USA*

Abstract
Purpose: The purpose of this study was to determine if accurate image-derived input functions (IDIF) can be measured from cardiac gated positron emission tomography (PET) images reconstructed using ordered subset expectation maximization–maximum *a posteriori* (OSEM-MAP) without further correction.
Procedures: IDIFs from the left ventricle were measured from cardiac gated PET images reconstructed using OSEM-MAP with computed tomography (CT)-based attenuation correction for five C57/BL6 mice. The accuracy of the IDIF was tested against blood samples using Bland–Altman analysis.
Results: Image-derived blood radioactivity concentration values were not significantly different from sampled blood values at two late time points as determined by a paired *t* test (P=0.97). Bland–Altman analysis revealed a mean difference of 0.06 μCi/ml (1%). Using kinetic analysis, the mean myocardial 2-deoxy-2-[^{18}F]fluoro-D-glucose uptake rate constant based on the IDIF was comparable to values reported in the literature based on physical blood sampling.
Conclusions: Accurate IDIFs can be obtained non-invasively. Although reconstruction times are increased, no further spillover corrections are necessary for IDIFs derived from gated, OSEM-MAP reconstructed images with attenuation correction.

Key words: Input function, Positron emission tomography, Small animal imaging, Spillover correction

Introduction

Tracer kinetic modeling is a commonly used method to quantitatively evaluate dynamic positron emission tomography (PET) data. The input function in this context refers to the amount of tracer in the blood available to the tissue and is required to estimate kinetic rate parameters of a compartmental model. The input function can be obtained invasively by direct arterial blood sampling, non-invasively by image-derived techniques, or by a combination of the two [1]. Catheter-based arterial blood sampling is the gold standard method for measuring the input function in mice [2]. However, it is particularly challenging to obtain the input function by catheterization in mice because of their small vessel size, fast metabolism, and small blood volume [3].

Input functions measured by region of interest (ROI) analysis of dynamic PET images are appealing because they minimize animal handling, avoid invasive catheterization procedures, and avoid the inherent time delay associated with arterial blood sampling. However, the intrinsic spatial

Correspondence to: Bijoy K. Kundu; *e-mail:* bkk5a@virginia.edu

resolution limitations of PET make this very challenging in mice. In particular, the partial volume (PV) effect can significantly restrict the absolute quantification of blood radioactivity measured and lead to underestimations of the image-derived input function (IDIF). In addition, a region located close to tissue containing high activity concentration will appear more intense than its actual value due to spillover (SP), leading to a time-dependent overestimation of the IDIF. Cardiac motion can cause image blurring, further confounding the effects of SP on the measured IDIF. To overcome these limitations, appropriate PV and SP corrections need to be applied.

A recently proposed method [4] attempts to overcome these limitations by simultaneously estimating the magnitude of SP and PV contaminating PET-derived input functions with compartmental model parameters. Reported "model-corrected" IDIFs correlated well with blood time–activity curves (TAC) obtained from sampling. However, due to the large number of parameters needed to be fitted simultaneously (between 15 and 18), we were not able to reliably replicate their results. Factor analysis (FA) is another approach that attempts to statistically separate the true blood TAC from that of the surrounding myocardium [5]. However, FA-derived input functions from the left ventricle in mice overestimated the measured input function at early time points, reflecting contamination by surrounding structures (i.e., myocardial wall and right ventricle). Furthermore, the impact of this contamination on the accuracy of estimated rate constants in various tissues has not been evaluated in mice. In this work, we show that the IDIF can be extracted from a left ventricular blood pool (LVBP) ROI without any further corrections when ordered subset expectation maximization–maximum a posteriori (OSEM-MAP) reconstructions and physiological gating are employed. We validate this method by comparing two late time-point 2-deoxy-2-[^{18}F]fluoro-D-glucose (FDG) blood radioactivity concentrations measured from LVBP ROIs of five mice with venous blood samples. As an additional justification of the IDIF accuracy derived from gated, OSEM-MAP-reconstructed images, we performed kinetic analysis in the heart using the three-compartment FDG model [6]. The net FDG uptake constant (K_i) estimated from the IDIF in the heart was compared to K_i values reported in literature using non-image derived input functions.

Materials and Methods

PET and CT Imaging

Five C57/BL6 mice (25-30 g), fasted overnight, were used in this study. Following the insertion of a tail-vein catheter, electrocardiogram (ECG) surface electrodes (Blue Sensor, Ambu Inc., Glen Burnie, MD, USA) were placed on both forepaws and the left hindpaw. Anesthetized (1–2% isoflurane in oxygen) mice were placed in the prone position on a custom designed portable tray designed to reproducibly mount on both the microcomputed tomography (CT) and PET scanners, facilitating accurate image co-registration. Sixty-minute dynamic PET scans (Focus 120, Siemens Molecular Imaging Inc., Knoxville, TN, USA) were performed where data acquisition was initiated a few seconds before the injection of 486–540 μCi FDG via the catheter. FDG was administered over the course of about 30 s, and the catheter line was immediately flushed with 100 μL of saline to clear the line and maximize FDG activity in the mouse. Physiological monitoring was performed with a Small Animal Instruments, Inc., model 1025L for PET (SAII, Inc., Stony Brook, NY, USA). This device was used for continuously monitoring heart rate, respiration, and core body temperature (rectal probe) while generating gate signals to time stamp the PET scanner data for subsequent retrospective reordering into heart-cycle based time bins. Following the PET scan, mice were immediately transported to the CT scanner [7], where a 10-min whole-body CT scan was acquired for attenuation correction [8].

Image Reconstruction

The list mode data were sorted into 23 dynamic frames and three cardiac-cycle time bins during the histogramming process. PET images were reconstructed with attenuation correction using an OSEM-MAP algorithm [9], which is part of the PET scanner software, with 12 OSEM 3D subsets, two iterations and 18 MAP iterations. For comparison, the data were also reconstructed using filtered back projection algorithm (FBP; ramp filter cutoff at the Nyquist frequency) with the same spatial resolution. Twenty-three dynamic frames were generated for each cardiac bin. The initial frames were set to be short in duration in order to capture rapidly changing radioactivity concentrations. The frames consisted of eleven 8-s frames, one 12-s frame, two 1-min frames, one 3-min frame, and eight 6-min frames. In order to obtain a sufficient number of pixels for extraction of the IDIF from the LVBP, a zoom factor of 2.16 was designated for all reconstructions. The reconstructed image was composed of 95 axial slices of thickness 0.79 mm with an in-plane voxel dimension of 0.4×0.4 mm (128×128 pixels). All PET images were corrected for dead time, physical radionuclide decay of FDG, and fluctuations in crystal detection efficiency. The count rates in the reconstructed images were converted to activity concentration (μCi/mL) using a system calibration factor obtained by PET scanning a sealed ^{68}Ge cylindrical phantom (Siemens Medical Solutions). All PET reconstructions were done on a Dell Dimension E521, running at 2.61 GHz with 3.43 Gb of RAM.

CT images were reconstructed with a 3D filtered back-projection algorithm using COBRA software (Exxim, Inc., Pleasanton, CA, USA). The CT reconstructed pixel size was 0.15×0.15×0.15 mm on a 320×320×384 image matrix but was down-sampled to match the PET spatial resolution upon image co-registration. CT-based attenuation correction was performed using the microPET scanner software.

Partial Volume Correction

To estimate the magnitude of the PV effect in the LVBP and myocardium, a Jaszczak Micro Deluxe hot rod phantom (Data Spectrum Corporation, Hillsborough, NC, USA) possessing six different rod sizes (1.2, 1.6, 2.4, 3.2, 4.0, and 4.8 mm) was filled with a known concentration of FDG and PET-scanned. The phantom image was reconstructed using both OSEM-MAP and FBP and corrected for attenuation (same protocol as described above). The average ROI-derived radioactivity concentrations

measured for the different sized rods were divided by the true activity concentration to obtain a recovery coefficient (RC) curve spanning the range of rod sizes. A unique RC curve was generated for each reconstruction method. The appropriate PV correction factors for the LVBP and myocardium were determined from the RC curve and applied to their respective time activity curves.

Obtaining the IDIF from PET images

IDIFs were measured by manually drawing small circular ROIs approximately 3 pixels in diameter (1.2 mm) on contiguous transverse planes on the last time frame of the dynamic PET dataset in the area corresponding to the LVBP and projecting these ROIs on all frames. This process was repeated on two to three transverse slices in which the LV cavity was visible so that an average blood TAC could be computed. All LVBP ROIs were drawn on the last cardiac time bin, corresponding to the phase of the heart in or near diastole, to minimize the amount of radioactivity SP from the myocardium into the blood pool. To correct for the PV effect in the LVBP, the IDIF was boosted by the RC obtained from the RC curve described above. No corrections were applied to account for FDG uptake by red blood cells.

Blood Sampling

Physical blood samples were obtained at 43 and 56 min post-FDG administration via a small incision in the distal tail. Approximately 40 μL of blood was collected in a pre-weighed capillary tube for each time point, while the anesthetized animal was being PET scanned. Excessive bleeding was prevented by applying gentle pressure for approximately 1 min. Each blood sample was weighed in an analytical balance (Pinnacle Series Model P-214, Denver Instruments, Denver, CO, USA), and the associated radioactivity was counted in a well counter cross-calibrated against the PET scanner. Radioactivity concentrations (in μCi/g) of the blood samples were determined by dividing the decay-corrected radioactivity measured in the well counter by the net weight of the blood in the capillary tube. Bland–Altman analysis was used to assess the agreement between image-derived and sampled blood radioactivity concentrations [10].

Kinetic Analysis

To further validate the accuracy of the IDIF, the net FDG influx constant (K_i) was computed in the myocardium by kinetic analysis. Kinetic transport rate constants of FDG uptake in the myocardium were estimated by the three-compartment FDG model using nonlinear regression [6] by a program written in MATLAB. From these estimated rate constants, K_i was computed in the heart and compared to values reported in the literature obtained by physical blood sampling.

Results

Figure 1 shows the hot rod phantom images reconstructed with MAP and FBP and the RC curves generated from them. For PET reconstructions using OSEM-MAP, the RC for the LV cavity was determined to be 0.92 based on previous magnetic resonance imaging (MRI) measurements of internal LV diameter of 3.3±0.2 mm (unpublished results). These

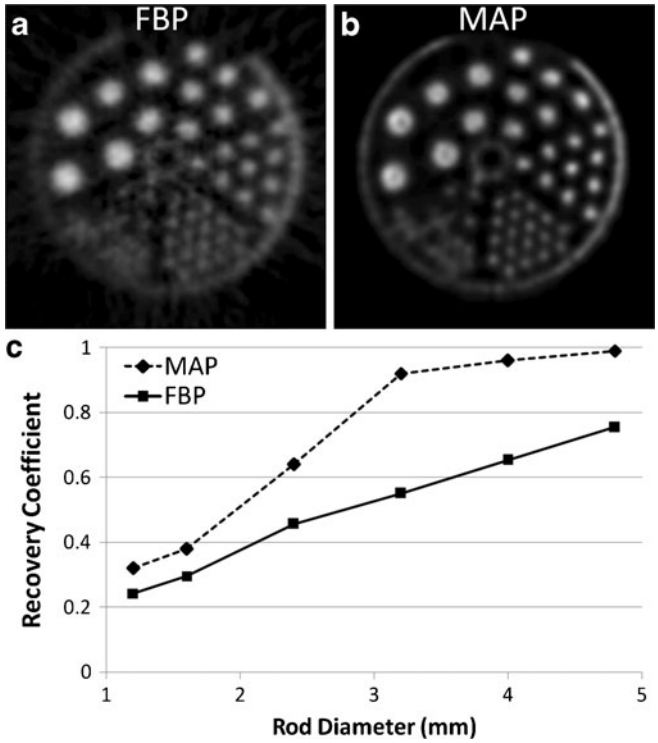

Fig. 1. Transaxial view of attenuation-corrected phantom images reconstructed with **a** FBP and **b** MAP and the recovery coefficient curves generated from them (**c**).

measurements are consistent with previously published values measured using ultrasound in mice of same age and background strain [11]. The RC was expected to approach one, since the dimension of the LV chamber is approximately twice the FWHM of the PET scanner [12]. For reconstructions using FBP, the RC for the LV cavity was determined to be 0.57. The RC for the myocardium at end diastole was determined to be 0.28 (based on the predetermined diameter of 0.9±0.1 measured by MRI).

Total reconstruction time using OSEM-MAP and FBP is approximately 34 h (30 min per frame per cardiac bin) and 8 min (7 s per frame per cardiac bin), respectively. Representative PET images of the same mouse acquisition reconstructed using both OSEM-MAP and FBP with and without cardiac gating are depicted in Fig. 2. All images shown are the last frame of the dynamic PET acquisition. OSEM-MAP reconstructed images (subpanels a and b) clearly show LVBP volumes that are well distinguished from the myocardium regardless of cardiac gating. FBP reconstructed images (subpanels c and d) are not able to achieve the same myocardium to blood pool contrast due to SP effects.

Figure 3 shows IDIFs derived from the reconstructed images depicted in subpanels a, c, and d of Fig. 2. The input function derived from the image reconstructed with FBP (black curve) shows significant SP contamination compared to the MAP-derived IDIF (gray curve). The IDIF derived

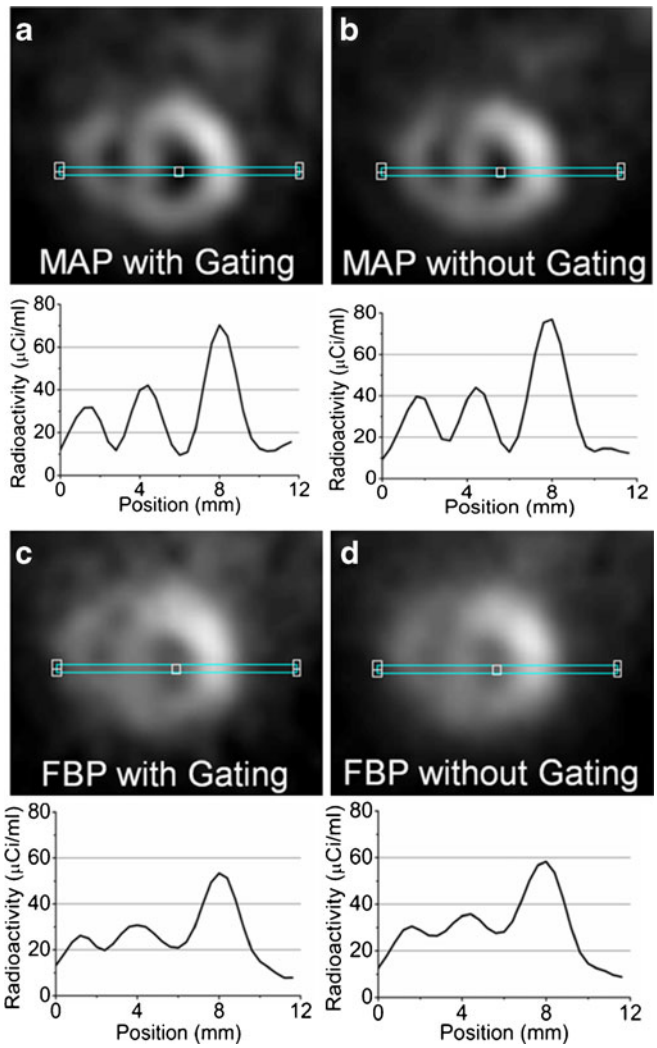

Fig. 2. Transverse FDG images of a mouse heart reconstructed using **a** OSEM-MAP with cardiac gating, **b** OSEM-MAP without cardiac gating, **c** FBP with cardiac gating, and **d** FBP without gating. Profiles through the transverse images are also shown. LVBP radioactivity concentrations are dependent on both image reconstruction algorithm and whether cardiac gating is employed. Cardiac-gated images show an improved contrast between the blood pool and the myocardium in diastole compared to non-gated images. The FBP images shown appear to be noisier than the corresponding OSEM-MAP images despite the fact that both images have the same resolution. Only gated OSEM-MAP images can be used to accurately measure LVBP radioactivity concentration.

from the non-gated FBP reconstruction shows the greatest amount of SP (dotted line). The peaks of the three curves are similar in magnitude due to PV correction and a lack of SP contamination at this time. The square and circle symbols, which represent the radioactivity concentrations of sampled blood taken at 43 and 56 min respectively, are in close agreement with time-matched activity concentrations of the MAP-derived input function.

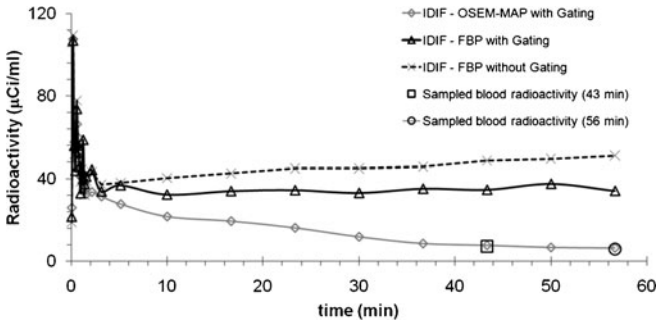

Fig. 3. Representative IDIFs for cardiac gated FBP and MAP reconstructions (*black and gray curves*, respectively) measured by a common ROI drawn in the region of the image corresponding to the LVBP. IDIF derived from non-gated FBP is shown (*dotted line*) to demonstrate the effect of not gating. CT-based attenuation and PV corrections were both applied. The *square* and *circular boxes* represent physically sampled blood activity concentrations taken at 43 and 56 min respectively, after FDG injection.

Figure 4 shows the agreement between the MAP image-derived and physically sampled blood radioactivity concentrations using a Bland–Altman plot. Bland–Altman analysis revealed a mean difference of 0.06 μCi/ml, which is approximately 1% of the average of all measured values. The precision (standard deviation of differences) was 0.14 μCi/ml. None of differences were outside the lower and upper limits of agreement (mean±1.96 SD), which were −0.22 and 0.34, respectively. As determined by the paired *t* test, image-derived blood radioactivity concentration values were not significantly different from sampled blood values (P=0.97).

The mean myocardial K_i (0.11±0.03) estimated from the gated, MAP-derived IDIF, agreed well with the reported myocardial K_i (0.14±0.06) [4] obtained using arterial blood samples, as the difference did not reach statistical significance on a Student's *t* test (p=0.19).

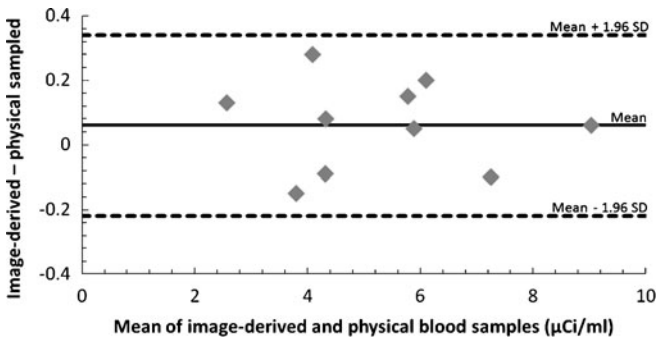

Fig. 4. Bland–Altman representation of the agreement between image-derived LVBP radioactivity (corrected for attenuation and partial volume effects) and physically sampled blood radioactivity in five mice. The mean difference was 0.06 μCi/ml (*solid line*) and the lower and uppers limits of agreement were −0.22 and 0.34, respectively (*dashed lines*).

Discussion

Kinetic modeling of PET data requires an input function along with tissue time–activity curves. Extracting the input function in mice from dynamic PET images is attractive because it bypasses many challenges associated with physical blood sampling. However, because the spatial resolution of PET is limited by factors, such as detector size, positron range, scatter, and cardiac motion, the activity concentration in an LVBP ROI will only be a fraction of the true radioactivity in the region. SP from surrounding myocardium will further reduce the accuracy, especially late after injection of FDG. The degree to which these effects influence image-derived activity concentrations is a function of LVBP diameter, the reconstructed image resolution, and the type of image reconstruction algorithm used [12].

Current techniques involving image-derived assessments of the input function are based primarily on non-cardiac gated, FBP reconstructed images. While FBP is fast and yields reliable quantitative results, it often results in poorer image quality and lower myocardium to LVBP ratios compared to MAP, as shown in Fig. 2. Iterative reconstruction algorithms offer better resolution recovery compared to FBP by accurate modeling of the system response, as shown in Fig. 2, and also demonstrated in various organ ROI measurements reported by Stout et al. [13]. However, even with iterative reconstructions, SP contamination from the myocardium to the LVBP was still reported to be significant without cardiac gating [13]. It has been expressed [3, 4, 13] but, to our knowledge, never demonstrated that using MAP-based reconstructions and segmenting list mode data into bins based on cardiac triggers is effective in minimizing SP from the myocardium to the LVBP. We have shown here that ROI-derived blood radioactivity concentrations agreed with physical samples taken at late time points, when SP effects are greatest. Furthermore, we have shown that the net FDG uptake (K_i) in the myocardium estimated from the three-compartment FDG model with the IDIF was not statistically different from reported values based on a physically sampled input function.

Although it would have been ideal to sample blood at the same location used to measure the image-derived activity concentrations (LV chamber), this would have required euthanizing the animal. It has been previously shown [4] that radioactivity from arterial blood is well approximated by venous blood for late time points, offering a less invasive alternative to acquiring a few discrete blood samples. Therefore, we sampled venous blood from the tail vein at two late time points to determine the accuracy of image-derived blood activity concentrations.

Differences between IDIFs derived from MAP and FBP reconstructions are greatest near the end of the scan (as shown in Fig. 3) due to time-dependent spillover contaminating the IDIF derived from the FBP-reconstructed image. There are appreciable differences in the early portion of the curves as well (around 20 min). Because we were measuring radioactivity concentrations from sampled venous blood obtained via the tail vein, we could not use this technique to validate the early portion of the IDIF. However, our data show good agreement between the IDIF and late blood samples, when the SP from the myocardium to the LVBP is most significant.

To avoid the effects of SP, some methods only derive the early portion of the input function from the image, while the latter part is obtained by blood samples [1]. Our results show that using OSEM-MAP with cardiac gating is effective in minimizing myocardial SP contribution to the IDIF at late time points. Reconstructions using OSEM-MAP lead to improved PET image spatial resolution through its advanced techniques that feature accurate system modeling, photon pair non-colinearity, and intercrystal scatter and penetration [9]. These techniques can help recover the loss of resolution from finite detector elements and drastically reduce both the amount of SP from the myocardium into the blood pool and also PV effects within the LV chamber. Eliminating cardiac motion by binning the PET data to the ECG further contributes to the reduction of SP contamination. By "freezing" the heart in the diastolic phase when the blood volume in the LV chamber is maximum, SP and PV effects are reduced in LV-derived input functions. Additional gating for respiratory motion only has a minimal effect on SP and PV effects in the LV chamber [14], thus was not employed in this study.

Although iterative reconstruction algorithms improve image quality due to their accurate modeling of data, they are time consuming. This technique may not be feasible for institutions that perform high-throughput imaging. However, if the appropriate time can be invested in the reconstruction process, this method can offer the ability to directly extract the IDIF without any further correction needed. In addition, future versions of OSEM-MAP may require less computation time.

Another potential limitation of this technique is its inability to correct for FDG uptake by red blood cells. Mice exhibit slower kinetics of FDG movement across the red blood cell membrane compared to humans, thereby delaying equilibrium and reducing the accuracy of whole blood as a surrogate marker for FDG in plasma in murine FDG studies [15]. To account for the time-dependent sequestering of FDG by red blood cells in mice, frequent blood samples must be taken, eliminating the possibility of a dynamic image based approach.

Fang et al. describe a technique to estimate the blood input function from a ROI-derived one containing significant contamination with zero or one late blood sample to account for red blood cell FDG uptake. Their one blood sample model-corrected input function (1-sample MCIF) corrects for the sequestering of FDG into red blood cells but does not account for any time dependence of this transport, thus assuming a constant fraction of red blood cell-associated FDG over time. Their 0-sample MCIF method does not correct for the sequestering of FDG into red blood cells. The K_i values computed in the myocardium by the 0- or the 1-sample method were not statistically different from the value estimated from invasive blood sampling with time-dependent

plasma correction [4]. Our average myocardial K_i value estimated from IDIFs with no correction for FDG red blood cell uptake was also not statistically different from this value, as indicated in "Results." Therefore, not accounting for sequestered FDG by red blood cells introduces small biases in downstream K_i values, but the magnitude of these biases does not exceed unreasonable amounts as demonstrated by the inability of the *t* test to detect a significant difference in the myocardial K_i estimates.

Conclusion

Employing cardiac gating and high-resolution iterative reconstruction algorithms improves PET image quality, reduces PV effects, and minimizes SP from the myocardium to the LVBP compared to non-gated, FBP images. We validated the ability to accurately measure blood pool radioactivity concentrations from the left ventricle in a normal mouse using image-derived techniques. Bland–Altman analysis revealed a negligible systematic bias between image-derived and physically sampled blood radioactivity concentrations for five mice studied. Furthermore, we have shown that the net FDG uptake in the myocardium determined using the IDIF with a three-compartment model was not statistically different from reported values obtained with a physically sampled input function. This technique should appeal to investigators who want to have the ability to measure the input function directly from PET images without further correction for quantitative dynamic PET studies in mice while avoiding the challenges associated with invasive blood sampling.

Acknowledgment. This work was supported in part by the Jeffress Grant, J-899 from the Jeffress Memorial Trust, the Partners fund from the University of Virginia Cardiovascular Research Center, and NIH grant 1R21HL102627 to BKK. The work was also supported in part by a gift provided by Philip Morris USA (the review and approval process was overseen by an External Advisory Committee without any affiliation with the University, PMUSA, or any other tobacco company. PMUSA funding for this work to SSB was based upon independent intramural and extramural reviews). The authors thank Gina Wimer for her assistance with the experiments.

Conflict of interest disclosure. The authors declare that they have no conflict of interest.

References

1. Shoghi KI, Welch MJ (2007) Hybrid image and blood sampling input function for quantification of small animal dynamic PET data. Nucl Med Biol 34:989–994
2. Wu HM, Sui G, Lee CC, Prins ML, Ladno W, Lin HD, Yu AS, Phelps ME, Huang SC (2007) In vivo quantitation of glucose metabolism in mice using small-animal PET and a microfluidic device. J Nucl Med 48:837–845
3. Laforest R, Sharp TL, Engelbach JA, Fettig NM, Herrero P, Kim J, Lewis JS, Rowland DJ, Tai YC, Welch MJ (2005) Measurement of input functions in rodents: challenges and solutions. Nucl Med Biol 32:679–685
4. Fang YH, Muzic RF Jr (2008) Spillover and partial-volume correction for image-derived input functions for small-animal 18F-FDG PET studies. J Nucl Med 49:606–614
5. Kim J, Herrero P, Sharp T, Laforest R, Rowland DJ, Tai YC, Lewis JS, Welch MJ (2006) Minimally invasive method of determining blood input function from PET images in rodents. J Nucl Med 47:330–336
6. Phelps ME, Huang SC, Hoffman EJ, Selin C, Sokoloff L, Kuhl DE (1979) Tomographic measurement of local cerebral glucose metabolic rate in humans with (F-18)2-fluoro-2-deoxy-D-glucose: validation of method. Ann Neurol 6:371–388
7. Stolin A, Pole D, Wojcik R, Williams MB (2006) Dual-modality scanner for small animal imaging. IEEE Nucl Sci Symp Conf Rec 4:2403–2407
8. Chow PL, Rannou FR, Chatziioannou AF (2005) Attenuation correction for small animal PET tomographs. Phys Med Biol 50:1837–1850
9. Qi J, Leahy RM, Cherry SR, Chatziioannou A, Farquhar TH (1998) High-resolution 3D Bayesian image reconstruction using the microPET small-animal scanner. Phys Med Biol 43:1001–1013
10. Bland JM, Altman DG (1999) Measuring agreement in method comparison studies. Stat Methods Med Res 8:135–160
11. Chin BB, Metzler SD, Lemaire A, Curcio A, Vemulapalli S, Greer KL, Petry NA, Turkington TG, Coleman RE, Rockman H, Jaszczak RJ (2007) Left ventricular functional assessment in mice: feasibility of high spatial and temporal resolution ECG-gated blood pool SPECT. Radiology 245:440–448
12. ME Phelps (2004) PET: molecular imaging and its biological applications, 1st edn. Springer, Berlin
13. Stout D, Kreissl MC, Hsiao-Ming W, Schelbert HR, Sung-Cheng H (2005) Left ventricular blood TAC quantitation with microPET imaging in mice using MAP, FBP and blood sampling. IEEE Nucl Sci Symp Conf Rec 5:2529–2531
14. Shoghi K, Rowland D, Laforest R, Welch M (2006) Characterization of spillover and recovery coefficients in the gated mouse heart for non-invasive extraction of input function in microPET studies: feasibility and sensitivity analysis. IEEE Nucl Sci Symp Conf Rec 4:2134–2136
15. Buxton DB (1999) Glucose permeability in nonprimate erythrocytes. J Nucl Med 40:2125–2126